PROCEEDINGS of the
23rd International Congress on Acoustics

9 to 13 September 2019 in Aachen, Germany

Optimization of leading-edge undulation of a NACA 65(12)-10 aerofoil for noise reduction and aerodynamic enhancement

Jung-Hoon KIM[1]; Kwing-So CHOI[1];
Giovanni LACAGNINA[2]; Phillip JOSEPH[2];
Seyed Mohammad HASHEMINEJAD[3]; Tze Pei CHONG[3];
Muhammad Farrukh SHAHAB[4]; Mohammad OMIDYEGANEH[4]; Alfredo PINELLI[4]
[1] University of Nottingham, UK
[2] University of Southampton, UK
[3] Brunel University, UK
[4] City, University of London, UK

ABSTRACT

Leading-edge undulations or tubercles of humpback whale flippers have been known as one of biomimetic technologies adaptable to flow control of aerofoils, particularly at post stall conditions. These leading-edge undulations are also known to reduce noise resulting from an interaction with on-coming turbulence. We have recently carried out a parametric study of a NACA 65(12)-10 aerofoil with a view to optimise the amplitude and the wavelength of leading-edge undulations for noise reduction and aerodynamic enhancement. A 3x3 test matrix composing of three amplitudes (h = 3%, 6% and 12% chord) and three wavelengths (λ = 10%, 20% and 30% chord) was used in the investigation, where lift, drag and noise were measured at the Reynolds number of 10^5. In this test, a turbulence-generating grid was installed at the inlet of the test section to increase the turbulence level in the freestream and to promote transition to turbulence near the leading edge of aerofoils without a need for a trip device. Within the test matrix considered, we found that the best improvement in $C_{L,max}$ is given with the greatest wavelength and amplitude, whereas the maximum noise reduction is obtained with the small wavelength and the large amplitude.

Keywords: Leading-edge undulation, NACA 65(12)-10, Lift, Drag, Noise

1. INTRODUCTION

Energy and environmental problems have become so critical to our current and future life that vast areas of scientists and engineers tackle these problems. Surely, these challenges are also significant motivations for most of researches in fluid mechanics. Among these, studies on low Reynolds flows around aero- or hydro-foils have long been carried out with this aim for the use of engineering applications such as propellers, windmills, helicopters, spoilers in automobiles, etc (1). Apart from the extensive studies on the generic shapes of an aerofoil associated with the boundary layer separation (2), many auxiliary methods have been devised to overcome the limit of their performances (3). These control methods can be categorised in different way, one of which divides them into active and passive ones depending on whether power are required for the control or not (1). Various active methods include plasma actuators for momentum addition (4) or streamwise vortical structure generation (5), synthetic jets (6), pneumatic blowing or suction (7), acoustic excitations (8), etc. Although the active methods have such advantages like comparatively high effectiveness and targeted controllability in time and space, passive control methods are attractive alternatives as they are because of the relative simplicity for the realization, less cost and no power requirement although it could have an adverse effect on the performance on off-design conditions for the actuators. The devices or mechanisms developed for passive control over low Reynolds number flows around foils include tripping wires to energise boundary layer for the promotion of transition to turbulence (9), Gurney flaps (10), vortex generators (11), etc. Nature inspires scientists or engineers in developing flow control methods one of which is tubercle or leading edge undulations discovered from the pectoral flipper of a Humpback whale.

The detailed morphology on Humpback whale's flippers was evaluated in (12) as an elliptically tapered, symmetrical aerofoil with leading edge undulations (LEU) and the measurements of the lift and drag of their test models were made in (13) which reported that the LEU delayed stall angle,

increased lift and decreased drag. On the contrary, when the LEU were applied to the test model of the same cross-section with that in (13) but of infinite span without taper, the maximum lift coefficient (C_{Lmax}) of the aerofoil with LEU was reduced or equal to the aerofoil with smooth leading edge although the lift in post-stall was dramatically increased (14). For most of studies where two dimensional infinite span of aerofoils were tested (15-17), the C_{Lmax} was not increased whereas stall was delayed compared to the corresponding smooth leading-edged aerofoils.

In addition to the effects of LEU on aerodynamic performances, their aeroacoustic effects have also been investigated. Adoption of LEU in the flat plate was shown in (18) to reduce aerofoil turbulence interaction noise and optimum wavelength of LEU was identified in (19) with regard to the transverse integral length scale. It is reported in (20) that peak and adjacent broadband noise coming from the aerofoil in the flow without artificial increase of turbulence were reduced by adopting LEU.

In our previous study, two dimensional infinite span of a NACA 65(12)-10 aerofoil, which is cambered and whose type of separation (21) is trailing edge separation at 10^5 of Reynolds number based on its chord length, was employed to investigate the effects of various cross sectional shapes with the amplitude and the wavelength of leading edge profile on the planform. As continuation of this work, the present study will demonstrate the results on the optimization of the two parameters in terms of aerodynamic and aeroacoustic performances.

2. Experimental Setup

2.1 Aerodynamic Force Measurement Facility

Aerodynamic force measurements were carried out in an open-return wind tunnel at the University of Nottingham. The dimension of the test section is 0.91 m wide x 0.75 m high and 1.5 m long. In these tests, a vertically installed aerofoil model was positioned at the mid-span, 0.1 m above the floor and 0.7 m downstream from the inlet of the test section. A schematic of the experimental set-up is shown in Figure 1. The aerofoil was connected to a force balance by an aluminium strut which was covered by an aerodynamic shaped fairing fixed to the wind tunnel floor. A circular plate in 150 mm diameter was attached to the bottom of the aerofoil, which was set in a circular hole provided by a 360 mm x 260 mm rectangular endplate. This allows the aerofoil to rotate through its transverse axis to change the angle of attack during the measurements. The top endplate, which is identical to the bottom endplate but without a hole, was fixed at the top of the aerofoil with a 2 mm gap. Each endplate had an elliptic leading edge with a major-to-minor axis ratio of 6 to 1. A 3-component force transducer (Kyowa, LSM-B-SA1, rated capacity: 10 N) was used to measure the drag and the lift on the aerofoil. The force balance was mounted on a turntable which was connected through a 2:1 gear to a stepping motor. The minimum angle of rotation of the turntable was 0.45 degree.

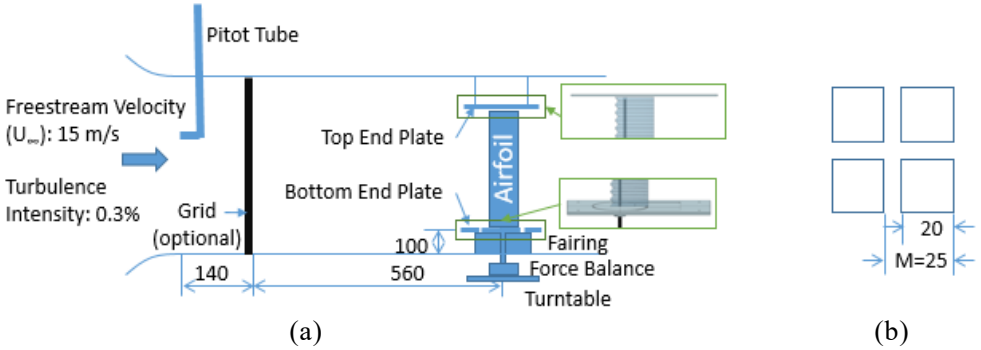

Figure 1 (a) A schematic of the experimental set-up (not to scale) and (b) the grid geometry. The unit for distance is mm.

In order to promote early transition of the boundary layer over an aerofoil, a perforated plate with a mesh size (M) of 25 mm was installed in a wind tunnel 0.56 m upstream of the rotational axis of the aerofoil models. The open-air ratio of this turbulence generating grid was 0.64. The mesh geometry is shown in Figure 1(b). The turbulence intensity and the longitudinal integral length scale at x/M = 22, where the aerofoil was installed, were 4.3% and 13 mm, respectively. The integral length scale was obtained using the method described in (22) and the ratio of nearly unity between the integral scale to

the plate thickness appears effective in promoting transition (23). Without the grid, the turbulence intensity at the same freestream speed was 0.3 %.

A NACA 65(12)-10 aerofoil with 100 mm chord length and 500 mm span, therefore the aspect ratio 5, was selected as a baseline case. The radius at the trailing edge was 0.5% of the chord length. Figure 2 shows the cross section at the peak (blue) and the trough (red) of the aerofoil with LEU. A solid and dashed green line are the camber lines at the peak and the trough section, respectively. This profile was selected in the current optimization as it showed the highest lift coefficient among the LEU profiles tested. For the optimization of wavelength and amplitude of the sinusoidal leading-edge undulation, 9 aerofoils with 3 variations in h (3%, 6% and 12% chord) and 3 variations λ (10%, 20% and 30% chord), were fabricated by a 3D printer, Zortrax M300 using Z HIPS (high impact polystyrene).

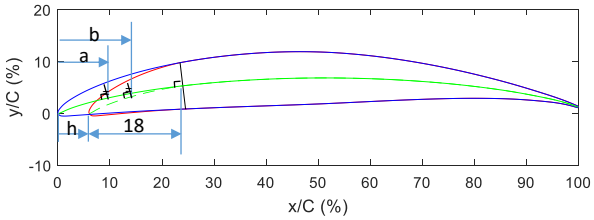

Figure 2 The cross sectional profile (blue) and the camber line (green) in the peak and the trough (red) profile with the camber line (dashed green) for the NACA 65(12)-10 with LEU.

2.2 Noise Measurement Facility

Acoustic measurements of the aerofoil have been carried on in the open jet wind tunnel facility of ISVR, at the University of Southampton. It is housed in an anechoic chamber of dimensions 8 m x 8 m x 8 m, whose walls are acoustically treated with glass-wool wedges to reach the lowest cut-off frequency of 80 Hz. A large nozzle, 500 mm high and 350 mm wide, was used so that the flow curvature and downwash deflection effects of an open wind tunnel can be miminised. The ratio between the geometrical angle α_{geom} and the effective one α_{eff} in the current experiment is about 1.35. Two side plates were located one chord-length downstream the nozzle to maintain the two-dimensionality of the flow. A detailed description of the facility can be found in (24).

An array of eight half-inch condenser microphones (B&K type 4189), located at a distance of 1.2 m at the mid span of the aerofoil, delivered the free-field noise measurements. The emission angles of the microphones, relative to the downstream direction of the jet axis, were in the range of 40 to 130 degrees. Finally, each noise measurement lasted for 20 s at the sampling frequency of 40 kHz.

3. Results

3.1 Aerodynamic Performance

Figure 3 shows the lift and drag coefficients as a function of the angle of attack of an aerofoil with leading-edge undulation with different wavelength λ. Note that the force coefficients are normalized by the planform area of each aerofoil. Experimental uncertainties are shown by error bars for the baseline case in Figure 3 (a). The uncertainties in the freestream velocity, force measurements and angle alignment are considered to be ±0.5% FS, ±0.3% FS and ±0.3°, respectively. The Root Sum Square method (25) was used to estimate the combined errors. The errors in the lift coefficient were estimated to be 0.8 % at α = 15.3° and 2.7% at α = 5.4°. On the other hand, the errors in the drag coefficients were 6.5% at α = 15.3° and 11% at α = 5.4°.

For aerofoils with LEU with a turbulence-generating grid installed in the wind tunnel (Figure 3 (a), (c) and (e)) C_L starts to deviate from baseline data at about α = 5°. For example, C_L of LEU with h/C = 3% and λ/C = 10% reduces after α = 5°, then increases near the maximum lift angle and reduces again after stall. Previous investigations on a similar LEU (14, 16) also indicated a reduction in C_L in pre-stall angles, which was due to the earlier separation around the trough section (17). C_L of LEU with h/C = 3% and λ/C = 20% or 30%, on the other hand, continue increasing up to the maximum lift angle. However, C_L of these aerofoils (h/C = 3%) do not outperform the baseline in post-stall angles. C_D curves of LEU with h/C = 3% collapse to the baseline data up to α = 18°, but a drag improvement can be found in post-stall angles. C_L and C_D behaviour with h/C = 6% (Figure 3 (c)) is similar to that with h/C = 3%. With h/C = 12% (Figure 3 (e)) C_L with λ/C = 10% reduces for all angles of attack. This may

implicate that there exists an optimum LEU configuration for C_{Lmax} within the range of wavelength and amplitude being tested. C_D of these aerofoils for α between 12° and 18° increases slightly as compared to that of the baseline, which may be caused by an earlier separation in the trough (17). With an increase in h/C (Figure 3 (e) and (f)), the difference in C_L at the maximum lift and post-stall angles became larger between different wavelengths tested, particularly with the grid.

The baseline result without grid (Figure 3 (b), (d) and (f)) is strongly influenced by laminar separation bubbles at the leading edge, giving a flat C_L curve between α = 10° to 16°. The stall angle is reduced without a grid, however. As compared to the baseline result, aerofoils with LEU are naturally "tripped" at the leading edge even without grid. Therefore, C_L and C_D curves without gird are similar to those with grid.

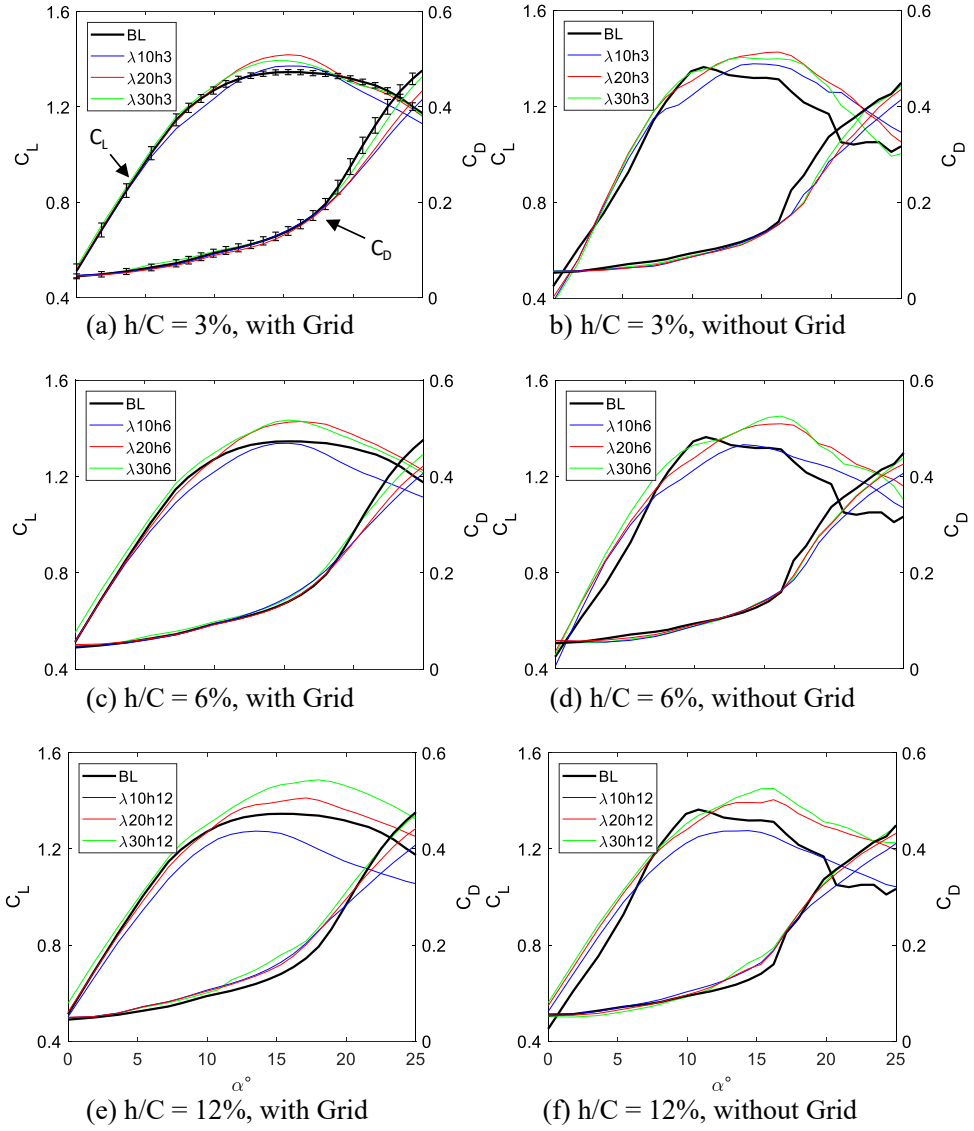

(a) h/C = 3%, with Grid

b) h/C = 3%, without Grid

(c) h/C = 6%, with Grid

(d) h/C = 6%, without Grid

(e) h/C = 12%, with Grid

(f) h/C = 12%, without Grid

Figure 3 Lift and drag coefficients of the aerofoils with the LEU: (a) h/C = 3%, with Grid; (b) h/C = 3%, without Grid; (c) h/C = 6%, with Grid; (d) h/C = 6%, without Grid; (e) h/C = 12%, with Grid; (f) h/C = 12%, without Grid.

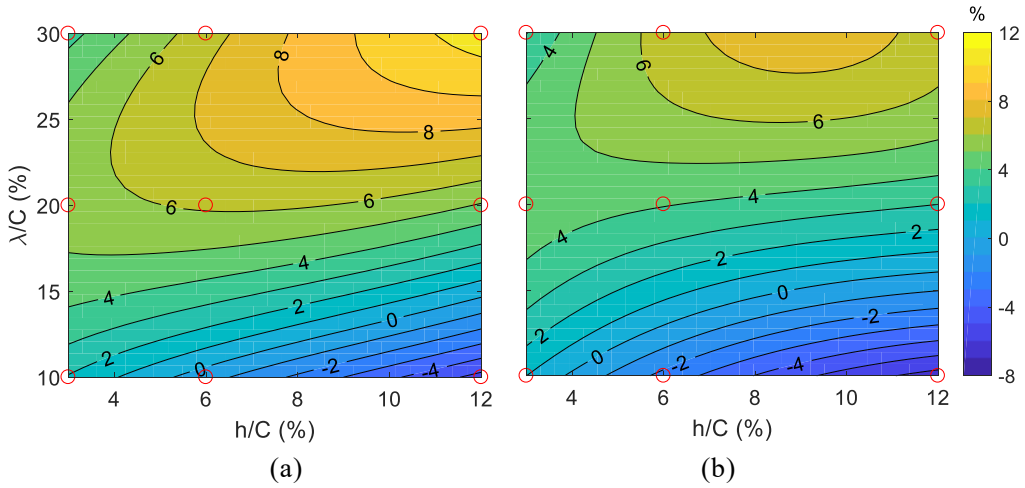

Figure 4 Contours of the differences in % values of the C_{Lmax} between the aerofoil with the LEU and the baseline normalized by that of the baseline: (a) With grid; (b) Without grid.

Figure 4 is a contour map to show the percentage change of C_{Lmax} with LEU, which are normalized by the baseline C_{Lmax} 'with grid' and 'without grid' in (a) and (b), respectively. The contour lines were obtained by interpolating 9 data points which are indicated by red circles. The figure shows that C_{Lmax} is increased by increasing λ/C of LEU, but the increment is insensitive to the change in h/C for λ/C < 20%. As λ/C increases further, C_{Lmax} increases with an increase in h/C. C_{Lmax} for an aerofoil with λ/C = 30% and h/C = 12% is increased by about 10 % with or without grid. The differences in maximum lift angle between the aerofoils with LEU and the baseline are shown in Figure 5. A similarity in behaviour between Figure 4 and Figure 5 suggests that an increase in C_{Lmax} by LEU is accompanied by an increase in the maximum lift angle. While there is no significant change by LEU with grid (Figure 5(a)), the maximum lift-angle is increased by up to 6 degrees by LEU without grid.

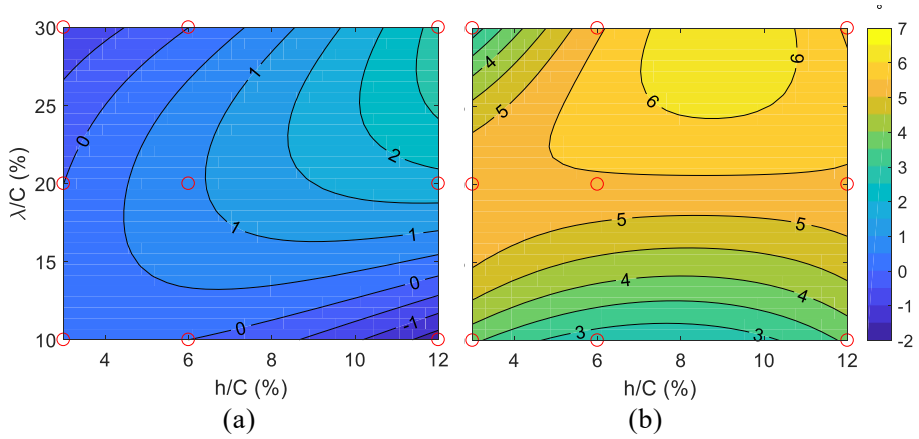

Figure 5 Contours for the maximum lift-angle change between the aerofoil with the LEU and the baseline: (a) With grid; (b) Without grid.

3.2 Aeroacoustic Performance

Figure 6 shows spectra of sound power level for the baseline aerofoil at three different effective angles at the freestream velocity of 20 m/s with and without the grid. The three effective angle of attack which are 3.7°, 14.8° and 22.3° represent pre-stall, stall and post-stall, respectively. The comparisons of the spectrums between with the grid (solid lines) and without the grid (dashed lines) indicate significant increase in the noise spectra by the interaction with the oncoming turbulent flow over the self-noise. The hump in the spectrum for 'α_{eff} = 3.7°, No Grid' (blue dashed) is also found in (26) which explains that the noise is caused by the interaction between Tollmien–Schlichting (T-S) wave convected downstream and the stationary laminar separation bubble on the aerofoil. Our previous studies also showed the separation bubble on the baseline aerofoil in this range of angle of attack. At α_{eff} = 14.8° near stall, the amplitudes

between 100 Hz and 1000 Hz were higher than those at α_{eff} = 22.3° beyond stall. Below 40 Hz, small increases are observed with the angle of attack. For the present test cases without the grid, our previous studies showed that separation / stall noise (27) corresponded to the noise spectrum in 40 Hz and 2000 Hz.

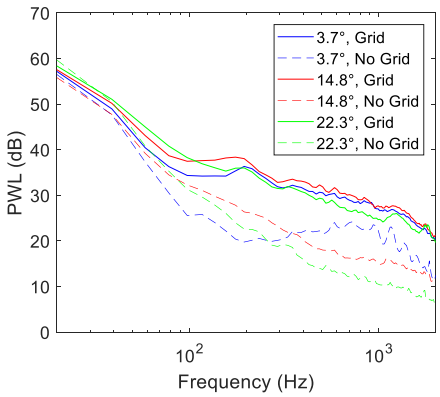

Figure 6 Sound Power Level for the baseline aerofoil at three representative angles of attack at the freestream velocity of 20 m/s with and without the grid.

Figure 7 shows the effects of LEU on the overall sound power level obtained from the integration of the spectra between 40 Hz and 2000 Hz. In each graph, variations of the overall sound power level with angle of attack were plotted for the LEU with 3 different wavelengths and the constant amplitude. For comparison, the variations of the noise from the baseline with the angle of attack are repeatedly shown in black in each figure. The noise data for the 'Grid' and 'No Grid' are designated by solid and dashed lines, respectively. For the cases of the 'Grid', the comparison of the noise profiles between these figures reveals that some values of h/C are effective in reducing the interaction noise with the oncoming turbulence and that the reductions are seen to increase with h/C although the reductions are not big enough to reach the noise levels of the case of 'No Grid'. Unlikely the cases for 'Grid', the noise profiles show complex shapes depending on the angle of attack. Between 0° and 8° where both the low frequency separation/stall (40 ~ 100 Hz) and the mid frequency T/S wave-separation bubble interaction noise (200 ~ 2000 Hz) dominate in the spectrum, the LEUs having λ/C = 20% and 30% with h/C = 6% and all the λ tested with h/C = 12% were effective in reducing the overall noise. Between 8° and 12° where highest L/D takes place, the overall noise appears to increase by the LEUs compared to the noise of the baseline. Beyond 18°, their effects on noise appear to have some relations with those on lift. This point may be indicated in Figure 8 which shows ΔOAPWL vs. ΔC_L of the aerofoils with LEU. ΔOAPWL and ΔC_L are the difference of OAPWL and C_L from the aerofoil with LEU to the baseline. The cross correlation coefficient between them was 0.63.

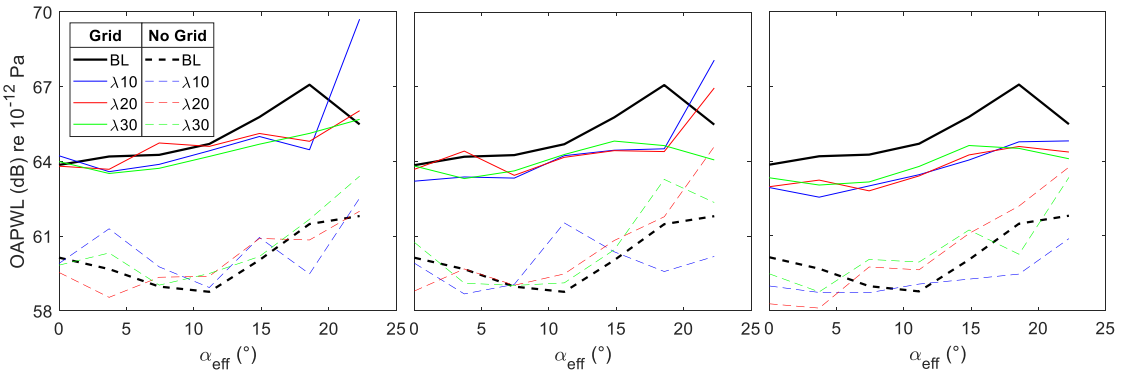

(a) h/C = 3% (b) h/C = 6% (c) h/C = 12%

Figure 7 Variations of overall sound power level with attack angle: (a) h/C = 3%; (b) h/C = 6%; (c) h/C = 12%. Blue, red and green lines designate λ/C = 10%, 20%, 30%, respectively, whereas those of the baseline in black are repeatedly shown for comparison. Solid and dashed lines denote for 'Grid' and 'No Grid', respectively. Integration was made between 40 and 2000 Hz.

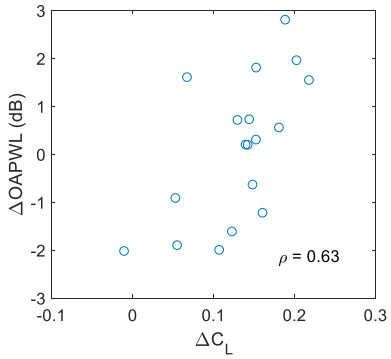

Figure 8 ΔOAPWL vs. ΔC_L for aerofoils with the LEU at over α_{eff} = 18° without the grid.

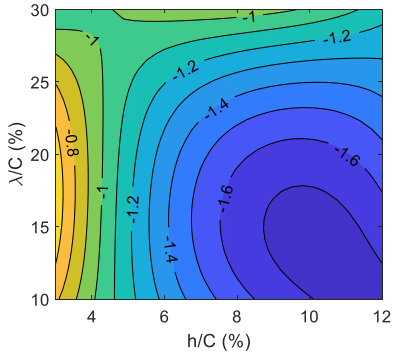

Figure 9 Contours of the noise reduction in dB by the LEU at α_{eff} = 15° with the grid.

Contours of the noise reduction by the leading edge undulation at α_{eff} = 15° with grid is plotted in Figure 9. It shows that optimal parameters are located at around λ/C = 15% and h/C = 10%. But it is not so meaningful because the level differences are less than 1 dB in the range of h/C larger than about 3.5%. Taking C_L into consideration, too low λ/C and high h/C may not be a good choice as the amount of noise reduction is not big enough. A compromise can be made to be λ/C = 30% and h/C = 6% considering drag near stall as well as C_{Lmax} and noise reduction.

4. CONCLUSIONS

For the continuation of previous studies on the optimization of the trough section of the leading edge undulation (LEU) of a NACA 65(12)-10, further explorations on the shape optimization of LEU were made in terms of the wavelength (λ) and the amplitude (h) by the experimental evaluation of their lifts, drags and aeroacoustic noises in low Reynolds number (~ 10^5) flow. Variations in their performances were also investigated in high freestream turbulence intensity (4.2%) flows. The test matrix for the parametric study was composed of λ/C = (10%, 20%, 30%) and h/C = (3%, 6%, 12%). With a turbulence-generating grid installed in the wind tunnel, the largest increase of the C_{Lmax} compared to the baseline was about 10% and the best improvement in $C_{L,max}$ was given with the greatest wavelength and amplitude. The increases of the C_Ls at post-stall angles became greater as h increased although the aerofoil with the LEU of high ratio of h/ λ underperformed the baseline in this range. The C_Ds in pre-stall angles increased as h increased and those in post-stall angles increased with λ. Without the grid, the increases of the C_L in post-stall angles by LEU were greater than those with the grid. The angles at C_{Lmax} of the aerofoils with LEU increased as the C_{Lmax} increased.

The effects on the aeroacoustic noise between 20 Hz and 2000 Hz which correspond to separation/stall noise were also evaluated. When the grid was installed, the LEUs reduced overall sound power level compared to the baseline by reducing turbulence interaction noise whose frequency range was between 150 Hz and 2000 Hz. Without the grid, their effects on noise also depended on the attack angle as well as the parameters of LEU. At low angle of attack, the LEUs with large h were effective in reducing T/S waves-separation bubble (T/S-SB) interaction noise. The effects on the noise in the lower frequency range than that of the T/S-SB interaction noise were not consistent. In α_{eff} between about 10° and 15° where the T/S-SB interaction noise disappeared, the noise components between 150 Hz and 2000 Hz grew larger by the LEU compared to the baseline. Beyond 15°, i.e. in post-stall, the effects of the LEU on the noise appeared to be correlated with those on lift coefficient.

For the cases with the grid, the overall noise map integrated between 20 Hz and 2000Hz at α_{eff}=15° which corresponds to the angle near the maximum lift may indicate that largest noise reduction be achieved by the LEU with high h and λ. However, taking lift into the consideration, the advantage of the largest noise reduction is reduced since the C_L increase around this parameter compared to baseline goes to nearly zero. A compromise can be made to be λ/C = 30% and h/C = 6% considering drag near stall as well as C_{Lmax} and noise reduction.

ACKNOWLEDGEMENTS

This study was supported by EPSRC (Grant Number EP/N018486/1) in the UK.

REFERENCES

1. Gad-el-Hak M. Flow control : passive, active, and reactive flow management. Cambridge : Cambridge University Press; 2000.
2. Abbott IH, Von Doenhoff AE. Theory of wing sections, including a summary of aerofoil data: Courier Corporation; 1959.
3. Houghton EL, Carpenter PW. Aerodynamics for engineering students: Elsevier; 2003.
4. Post ML, Corke TC. Separation control on high angle of attack aerofoil using plasma actuators. AIAA J. 2004;42(11):2177-84.
5. Jukes TN, Segawa T, Furutani H. Flow Control on a NACA 4418 Using Dielectric-Barrier-Discharge Vortex Generators. AIAA J. 2013;51(2):452-64.
6. Amitay M, Smith DR, Kibens V, Parekh DE, Glezer A. Aerodynamic flow control over an unconventional aerofoil using synthetic jet actuators. AIAA J. 2001;39(3):361-70.
7. Dannenberg RE, Weiberg JA. Section Characteristics of a 10.5-Percent-Thick Aerofoil with Area Suction as Affected by Chordwise Distribution of Permeability. 1952.
8. Zaman KBMQ, Barsever A, Mangalam SM. Effect of Acoustic Excitation on the Flow over a Low-Re Aerofoil. J Fluid Mech. 1987;182:127-48.
9. Schlichting H. Boundary-layer theory: Springer; 1974.
10. Jeffrey D, Zhang X, Hurst DW. Aerodynamics of Gurney flaps on a single-element high-lift wing. J Aircraft. 2000;37(2):295-301.
11. Storms BL, Jang CS. Lift Enhancement of an Aerofoil Using a Gurney Flap and Vortex Generators. J Aircraft. 1994;31(3):542-7.
12. Fish FE, Battle JM. Hydrodynamic-Design of the Humpback Whale Flipper. J Morphol. 1995;225(1):51-60.
13. Miklosovic DS, Murray MM, Howle LE, Fish FE. Leading-edge tubercles delay stall on humpback whale (Megaptera novaeangliae) flippers. Phys Fluids. 2004;16(5):L39-L42.
14. Johari H, Henoch C, Custodio D, Levshin A. Effects of leading-edge protuberances on aerofoil performance. AIAA J. 2007;45(11):2634-42.
15. Custodio D, Henoch CW, Johari H. Aerodynamic Characteristics of Finite Span Wings with Leading-Edge Protuberances. AIAA J. 2015;53(7):1878-93.
16. Hansen KL, Kelso RM, Dally BB. Performance Variations of Leading-Edge Tubercles for Distinct Aerofoil Profiles. AIAA J. 2011;49(1):185-94.
17. Zhang MM, Wang GF, Xu JZ. Experimental study of flow separation control on a low-Re aerofoil using leading-edge protuberance method. Exp Fluids. 2014;55(4).
18. Haeri S, Kim JW, Narayanan S, Joseph P, editors. 3D calculations of aerofoil-turbulence interaction noise and the effect of wavy leading edges. 20th AIAA/CEAS Aeroacoustics Conference; 2014.
19. Chaitanya P, Joseph P, Narayanan S, Vanderwel C, Turner J, Kim JW, et al. Performance and mechanism of sinusoidal leading edge serrations for the reduction of turbulence-aerofoil interaction noise. J Fluid Mech. 2017;818:435-64.
20. Hansen K, Kelso R, Doolan C. Reduction of Flow Induced Aerofoil Tonal Noise Using Leading Edge Sinusoidal Modifications. Acoust Aust. 2012;40(3):172-7.
21. Gault DE. A correlation of low-speed, aerofoil-section stalling characteristics with Reynolds number and aerofoil geometry. NACA TN39631957.
22. Kurian T, Fransson JHM. Grid-generated turbulence revisited. Fluid Dynamics Research. 2009;41(2):021403.
23. Nakamura Y, Ozono S. The Effects of Turbulence on a Separated and Reattaching Flow. J Fluid Mech. 1987;178:477-90.
24. Chong TP, Joseph PF, Davies POAL. Design and performance of an open jet wind tunnel for aero-acoustic measurement. Appl Acoust. 2009;70(4):605-14.
25. Moffat RJ. Describing the Uncertainties in Experimental Results. Exp Therm Fluid Sci. 1988;1(1):3-17.
26. Chong TP, Joseph PF. An experimental study of aerofoil instability tonal noise with trailing edge serrations. J Sound Vib. 2013;332(24):6335-58.
27. Brooks TF, Pope DS, Marcolini MA. Aerofoil self-noise and prediction. 1989.